Modeling and Impedance Analysis of a Turbine-Generator-Rectifier System with Electromechanical Dynamic Interactions in More Electric Aircraft

Qing Lin[1], Bo Wen[1], Rolando Burgos[1], John Noon[2]
[1]Center for Power Electronics Systems (CPES)
Virginia Polytechnic Institute and State University
Blacksburg, VA, USA
[2]Moog Inc, Blacksburg, VA, USA
Email: qingl19@vt.edu, wenbo@vt.edu, rolando@vt.edu, njohn14@vt.edu

Abstract— **More electric aircraft concept has been a trend in the aircraft industry to tackle the challenge of reducing cost and weight, reducing environmental emissions, and increasing fuel efficiency. This increase in onboard electric power installation has brought challenges in the design and operation of aircraft electrical power systems. Onboard electric power is generated by turbine-driven generators and transferred to multiple loads through a dc distribution system. To ensure the electrical system's normal operation during the whole flying profile, it is important to understand whether harmonics are passed through electromechanical coupling, since the electrical system is tightly coupled with the mechanical system through the generators. By examining generator output impedance, this paper found that the impact of the shaft dynamics on the electrical power system stability is mitigated by the generator rectifier.**

Keywords—More electric aircraft, small-signal impedance modeling, stability analysis, electromechanical dynamics

I. INTRODUCTION

Electric aircraft propulsion technologies have gained significant attention in the aviation industry for their potential to reduce emissions, increase fuel efficiency and reduce noise for commercial airplanes [1,2]. Achieving these benefits would be a vital step towards environmental sustainability. However, the development of all-electric aircraft is still limited by the current battery and maintenance technologies. More electric aircraft (MEA) with hybrid propulsion is developed to bridge the gap between the current fuel-powered aircraft and future all-electric aircraft. It uses electric motors powered by gas turbines and transfers power to other locations of the airplane through the onboard electrical power system to provide distributed propulsion, i.e., the tail fan motor [3, 4]. Power electronics converters play a significant role in power transfer in the aircraft electrical power system. With a high penetration of power electronics and the increase of electrical power level, potential stability issue resulted from the cross-domain dynamic interaction between the mechanical and the electrical system need to be paid attention to [5].

High voltage dc (HVDC) distribution has been promoted in MEA power system architecture development for its advantage of increasing efficiency and better voltage regulation over the conventional ac distribution. A turbine-generator-rectifier system feeding a dc bus with multiple loads is studied in this paper, the configuration of which is shown in Fig. 1 [6]. This paper utilizes the impedance-based small-signal stability analysis method, which has been used in more electric aircraft power system stability analysis, however, up to authors' knowledge, the impact of mechanical disturbances has not yet been considered [7-9]. By studying the rotor dynamics' impact on the output impedance of the turbine-generator-rectifier system to assess the mechanical dynamics' impact on the stability condition of the electrical system, it is found that the rotor dynamics of the turbine is masked by the rectifier; therefore, it does not cause stability problem to the pre-tuned system.

The rest of this paper is organized as followed. Section II introduces the power stage and control design of the turbine-generator-rectifier system. Section III presents the small-signal model derivation and analyzes the impedance with and without considering the mechanical dynamics. Section IV shows the impact of distributed propulsion ratio on the results obtained in Section III. Section V summarizes this paper.

II. MODELING AND CONTROL SCHEME

The permanent magnet synchronous generator (PMSG) is rated at 1MW, the dc bus voltage is rated at 1kV, and the active front end (AFE) output capacitor is chosen to be 5mF. The generator stator inductance also functions as the boost inductor
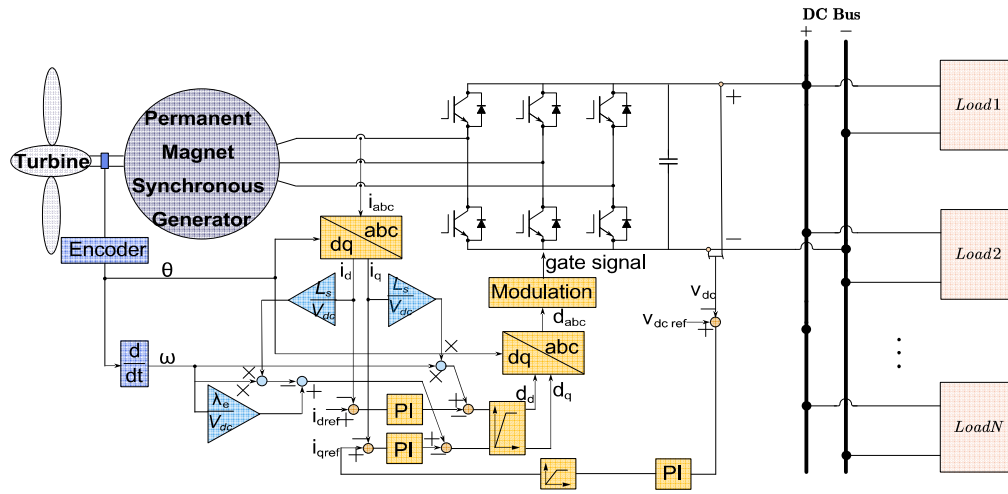
Figure 1 Onboard dc distribution system

Figure 2 Average model in DQ frame

Figure 3 Converter dc side impedance shaping
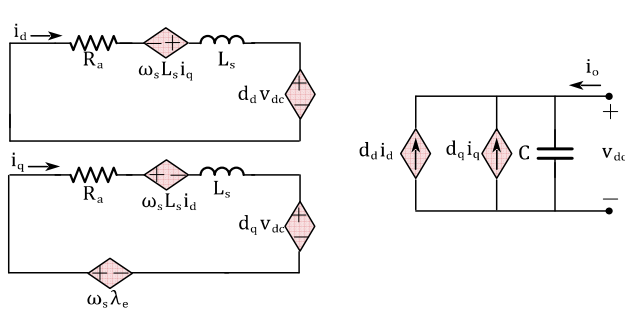
of the rectifier. The switching model of the rectifier is built in Simulink with a switching frequency of 60kHz. Multiple loads, including motor drive, battery converter, and housekeeping loads, are connected to the dc bus through power electronics interface, the rated power of which are 1MW, 100kW, and 100kW respectively [10].

The switching model of the generator-rectifier in Fig. 1 can be converted to an average model in the DQ frame by averaging the electrical variables in one switching cycle and applying Park's transformation. The d axis is aligned with the rotating magnetic field, and the q axis is aligned with the motor torque. The average model in the DQ frame is shown in Fig. 2, which can also be written as Equation (1) ~ (3). R_a and L_s are the equivalent winding resistance and inductance of the PMSG in DQ frame, and λ_e is the voltage constant.

$$d_d v_{dc} = -(R_a + sL_s)i_d + \omega_s L_s i_q \quad (1)$$

$$d_q v_{dc} = -(R_a + sL_s)i_q - \omega_s L_s i_d + \omega_s \lambda_e i_d \quad (2)$$

$$d_d i_d + d_q i_q + i_o = C\frac{dv_{dc}}{dt} \quad (3)$$

As shown in Figure 1, a dual-loop vector control strategy is applied, where the outer loop regulates the dc bus voltage with a proportional-integra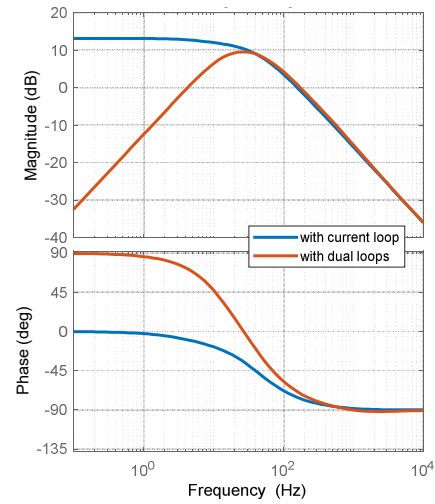l (PI) controller and provides the reference value for i_q. The reference of i_d is set as 0 to achieve unity power factor control. Both current loops utilize PI controllers and include the current and speed decoupling terms. Without considering the mechanical dynamics, the output impedance of the generator-rectifier system is mainly shaped by its controller and output capacitor. Fig. 3 gives an example of the dc side impedance of a rectifier with capacitor. The blue curves show the case with only the current loop and the red curve shows the case with both current loop and voltage loop. If the rectifier is only designed with a current loop, in the low-frequency range, it appears to be a constant power source with gain equal to V_{dc}^2/P , and phase equal to 0 because the converter supplies power to the dc bus. In the mid-frequency to high-frequency range, the converter impedance is mainly shaped by the output capacitor. It has a 20dB/dec slope and -90° phase at high frequency. If the converter is designed to regulate the dc bus voltage, the output impedance can be calculated using,

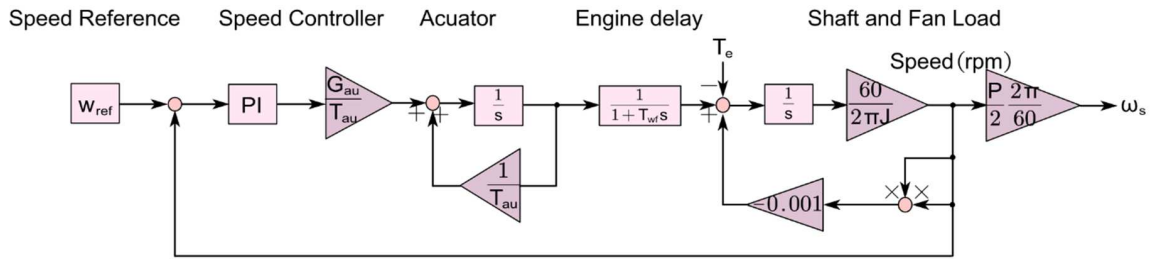$$Z_{vo} = \frac{Z_{cu}}{1 + T_v} \quad (4)$$
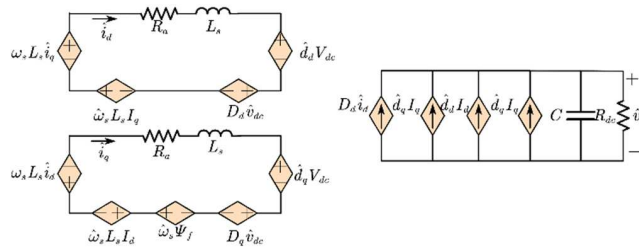
3519

Figure 4 Shaft dynamics model

Figure 5 Small-signal model of turbine-generator-rectifier system

where Z_{cu} is the converter impedance with only the current loop and T_v is the voltage loop open-loop gain. At low frequency, $T_v = K/s$ so the gain of Z_{vo} is attenuated compared with Z_{cu}, while the phase is pushed up to 90°. This is shown in the red curve in Fig. 3.

For a general aerospace electro-mechanical system, the mechanical dynamics include the gas turbine dynamics and mechanical drivetrain dynamics, i.e., damping, inertia and stiffness. In this work, the mechanical drivetrain dynamics are ignored due to the limit of resource, and only the prime mover speed controller dynamics is considered. The turbofan shaft is emulated using the advanced geared turbofan engine system model AGTF30 which represents a hypothetical 30-kilo lbf thrust class geared turbofan engine [11]. In the convenience of further analysis, the original AGTF30 model is simplified, as shown in Fig. 4. The speed controller is tuned that it has a same speed response of torque change as the original model to accurately represent the original shaft dynamics.

The simplified model is mainly composed of the speed controller, the actuator, engine delay, and shaft with fan load. The low-pressure shaft is the mechanical and electrical interface where the generator load is a resistant torque labeled as T_e, which can be calculated using Equation (5), where P_o is the number of poles. The output signal is the stator electrical frequency ω_s, which is the input signal of the generator.

$$T_e = \frac{P_o}{2} \lambda_e i_q \qquad (5)$$

III. SMALL-SIGNAL MODEL AND IMPEDANCE DERIVATION

The impedance-based stability criterion is used to assess the stability condition of the dc distribution system [7, 8]. For a dc system, the ratio between the source impedance and load
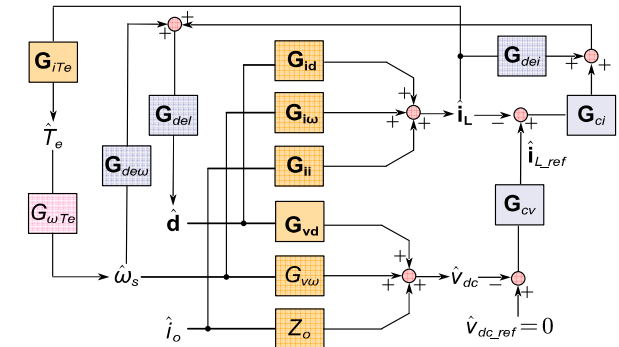

Figure 6 Block diagram of the system linear dynamics model

impedance Z_s/Z_L is defined as the "minor loop gain" of the whole feedback control system. Nyquist stability criterion can then be applied to the minor loop gain for stability assessment. Here the rectifier regulates the dc bus voltage, so it is considered as the source subsystem. The other components are grouped as the load subsystem. To obtain the minor loop gain, it is necessary to derive the small-signal impedance of both the source subsystem and load subsystem. Since the shaft dynamics couple with the electrical system through the generator, the output impedance of the source subsystem is of the main interest here. By linearizing the average model at the rated operating point, the small-signal model circuit can be derived, as is shown in Fig. 5.

Fig. 6 is the turbine-generator-rectifier system linear dynamics model in block diagram. The power stage transfer functions are shown in the orange blocks, with the input variables duty cycle $\hat{\mathbf{d}}$, stator electrical frequency $\hat{\omega}_s$, and load side perturbed current $\hat{i}_o$, and state variables, inductor current $\hat{\mathbf{i}}_L$, dc bus voltage $\hat{v}_{dc}$, and electromagnetic torque $\hat{T}_e$. $\mathbf{G}_{id}$, $\mathbf{G}_{i\omega}$, $\mathbf{G}_{ii}$, $\mathbf{G}_{vd}$, $\mathbf{G}_{v\omega}$, $\mathbf{Z}_o$, and $\mathbf{G}_{iTe}$ are the open-loop transfer functions, which are derived from the open-loop power stage small-signal model in Fig. 5. $\mathbf{G}_{id}$ is the transfer function matrix from duty ratio to inductor current; $\mathbf{G}_{vd}$ is the transfer function matrix from duty ratio to output dc voltage; $\mathbf{G}_{i\omega}$ is the transfer function matrix from electrical speed to inductor current; $\mathbf{G}_{v\omega}$ is the transfer function matrix from electrical speed to output dc voltage; $\mathbf{G}_{ii}$ is the transfer function matrix from dc side current to the inductor current; $\mathbf{Z}_o$ is the open-loop output impedance. $\mathbf{G}_{\omega Te}$ is the transfer function matrix from electrical torque to the electrical speed, which is derived from the small-signal model of the turbofan shaft model and its control in Fig.

3520

4. Blocks in blue represent the converter control, including the voltage controller $\boldsymbol{G}_{cv}$, inner current controller $\boldsymbol{G}_{ci}$, decoupling terms $\boldsymbol{G}_{dei}$ and $\boldsymbol{G}_{de\omega}$, and control delay $\boldsymbol{G}_{del}$ in second-order approximation, as are shown in Equation (6)~(10).

$$\mathbf{G}_{cv} = \begin{bmatrix} 0 \\ \dfrac{k_{pv}s + k_{iv}}{s} \end{bmatrix} \tag{6}$$

$$\mathbf{G}_{ci} = \begin{bmatrix} -\dfrac{k_p s + k_i}{s V_{dc}} & 0 \\ 0 & -\dfrac{k_p s + k_i}{s V_{dc}} \end{bmatrix} \tag{7}$$

$$\mathbf{G}_{dei} = \begin{bmatrix} 0 & \dfrac{\omega_s L_s}{V_{dc}} \\ -\dfrac{\omega_s L_s}{V_{dc}} & 0 \end{bmatrix} \tag{8}$$

$$\mathbf{G}_{de\omega} = \begin{bmatrix} \dfrac{I_q L_s}{V_{dc}} \\ \dfrac{\lambda_e - I_d L_s}{V_{dc}} \end{bmatrix} \tag{9}$$

$$\mathbf{G}_{del} = \begin{bmatrix} \dfrac{1 - 0.5 s T_{del}}{1 + 0.5 s T_{del}} & 0 \\ 0 & \dfrac{1 - 0.5 s T_{del}}{1 + 0.5 s T_{del}} \end{bmatrix} \tag{10}$$

The closed-loop output impedance Z_{CL} can be solved as,

$$Z_{CL} = \frac{\hat{v}_{dc}}{\hat{\imath}_o} \tag{11}$$

Z_{CL} can also be written as Equation (4), with

$$Z_{cu} = Z_o + \mathbf{M}\mathbf{G}_{ii} \tag{12}$$

$$T_v = (\mathbf{G}_{vd} + \mathbf{M}\mathbf{G}_{id})\mathbf{G}_{del}\mathbf{G}_{ci}G_{cv} \tag{13}$$

$\mathbf{M}$ is a predefined matrix. Without considering the rotor dynamics, that is assuming $\hat{\omega}_s = 0$, $\mathbf{M}=\mathbf{M}_1$, where

$$\mathbf{M}_1 = \left(\mathbf{I} - \mathbf{G}_{id}\mathbf{G}_{del}(\mathbf{G}_{dei} - \mathbf{G}_{ci})\right)^{-1} \cdot \\ \mathbf{G}_{vd}\mathbf{G}_{del}(\mathbf{G}_{dei} - \mathbf{G}_{ci}) \tag{14}$$

If considering rotor dynamics, $\mathbf{M}=\mathbf{M}_2$, where

$$\mathbf{M}_2 = \Big(\mathbf{I} - \big(\mathbf{G}_{id}\mathbf{G}_{del}\big(\mathbf{G}_{de\omega}\mathbf{G}_{Te} + (\mathbf{G}_{dei} - \mathbf{G}_{ci})\big) + \\ G_{i\omega}\mathbf{G}_{Te}\big)\Big)^{-1} \cdot \big(\mathbf{G}_{vd}\mathbf{G}_{del}\big(\mathbf{G}_{de\omega}\mathbf{G}_{Te} + (\mathbf{G}_{dei} - \\ \mathbf{G}_{ci})\big) + G_{v\omega}\mathbf{G}_{Te}\big) \tag{15}$$

where $\mathbf{G}_{Te}$ is defined as Equation (16),

$$\mathbf{G}_{Te} = \mathbf{G}_{iTe}\mathbf{G}_{\omega Te} \tag{16}$$

By comparing $\mathbf{M}_1$ and $\mathbf{M}_2$, the difference only lies in three terms, $\mathbf{G}_{de\omega}\mathbf{G}_{Te}$, $G_{v\omega}\mathbf{G}_{Te}$, and $\mathbf{G}_{i\omega}\mathbf{G}_{Te}$. Therefore, it is necessary to check the four related transfer function matrices $G_{v\omega}$, $\mathbf{G}_{i\omega}$, $\mathbf{G}_{Te}$, and $\mathbf{G}_{de\omega}$.

$G_{v\omega}$ is the transfer function matrix from electrical speed to output dc voltage, which reflects the speed perturbation's
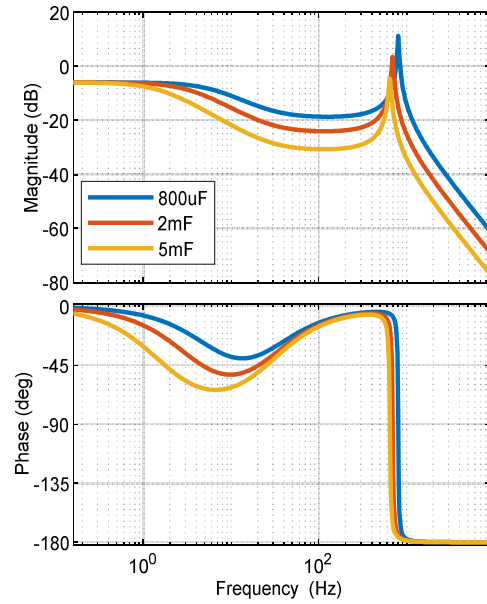

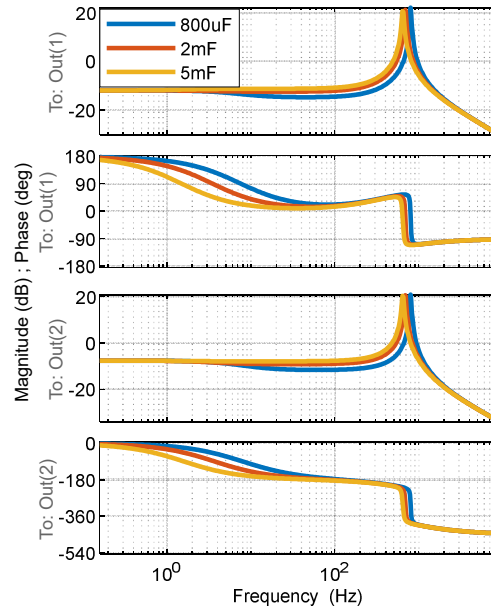Figure 7 Bode plot of $G_{v\omega}$

Figure 8 Bode plot of $\mathbf{G}_{i\omega}$

impact on the output dc voltage. $G_{v\omega}$ is shown in Fig. 7 with different output dc capacitor value. When the rectifier output capacitor is 5 mF, the gain below 100Hz is around -8dB, indicating that the speed perturbation has a small impact on the dc bus voltage. The gain of $G_{v\omega}$ in the whole frequency range reduces with the increase of capacitance, meaning that a larger output capacitor will reduce the impact of speed perturbation on dc voltage. There is a real zero z_1, a real pole p_1 and a double pole in $G_{v\omega}$. The approximation of z_1, p_1 and the resonant frequency ω_n of the double pole is shown in Equation (17) ~ (19). p_1 is located at very low frequency which results in a decrease of the magnitude at low frequency.

3521

$$z_1 = -\frac{R_a}{L_s}\left(1 + \frac{1}{1 + \frac{\lambda_e D_q}{I_q D_d L_s}}\right) \quad (17)$$

$$p_1 \approx \frac{R_s}{L_s + \frac{C\omega_s{}^2 L_s{}^2}{D_d{}^2 + D_q{}^2}} \quad (18)$$

$$\omega_n = \sqrt{\omega_s{}^2 + \frac{D_d{}^2 + D_q{}^2}{CL_s}} \quad (19)$$

$\mathbf{G}_{i\omega}$ is the transfer function matrix from electrical speed to inductor current, which reflects the inductor current response to the speed perturbation. The gain at low frequency in DQ frame are -14dB and -10dB, respectively, as shown in Fig. 8. This indicates that the speed perturbation has a small impact on the inductor current. The poles of $G_{i\omega}$ are the same as those of $G_{v\omega}$. The zeros of $G_{i\omega}$ are shown below, where z_2 is of $G_{i\omega d}$ and z_3 is of $G_{i\omega q}$. The real zeros and real pole locate at similar low frequency point therefore the magnitude maintains at a low value at low frequency.

$$z_2 = \frac{-\lambda_e \omega_s \pm \sqrt{(\lambda_e \omega_s)^2 + \frac{4D_q I_q (\lambda_e D_d - I_q D_q L_s)}{C}}}{2I_q L_s} \quad (20)$$

$$z_3 = \frac{I_q L_s{}^2 \omega_s \pm \sqrt{(I_q L_s \omega_s)^2 - \frac{4\lambda_e L_s D_d (\lambda_e D_d - I_q D_q L_s)}{C}}}{2\lambda_e L_s} \quad (21)$$

$\mathbf{G}_{Te}$ is the multiplication of $\mathbf{G}_{iTe}$ and $\mathbf{G}_{\omega Te}$. $\mathbf{G}_{\omega Te}$ reflects the turbine shaft dynamics. Since $\mathbf{G}_{iTe}$ is 0 in d axis, only the component of $\mathbf{G}_{Te}$ at q axis G_{Te_q} matters. As shown in Fig. 9, at low frequency range, the gain of G_{Te_q} is around -30dB. There are three zeros, z_4, z_5, z_6, two real poles p_2, p_3 and a double pole in $\mathbf{G}_{Te}$, derived as Equation (22) ~(27). ω_{n2} is the resonant frequency of the double poles.

$$z_4 = 0 \quad (22)$$

$$z_5 = -\frac{1}{T_{au}} \quad (23)$$

$$z_6 = -\frac{1}{T_{wf}} \quad (24)$$

$$p_2 \approx -\frac{1}{T_{au}} \quad (25)$$

$$p_3 \approx -\frac{1}{T_{wf}} \quad (26)$$

$$\omega_{n2} \approx \sqrt{\frac{G_{au} k_{is}}{J\frac{2\pi}{60}}} \quad (27)$$

where T_{au} is the actuator time constant, G_{au} is the actuator gain, T_{wf} is the engine delay time constant, J is the turbine inertia, and k_{is} is the turbine speed controller integrator coefficient. It can be seen that z_5 and p_2, z_6 and p_3 cancel with each other. ω_{n2} locates at low frequency, which causes the gain to drop at low frequency.

$\mathbf{G}_{de\omega}$ is used to attenuate the coupling terms, so it further attenuates the effect of $\mathbf{G}_{Te}$.
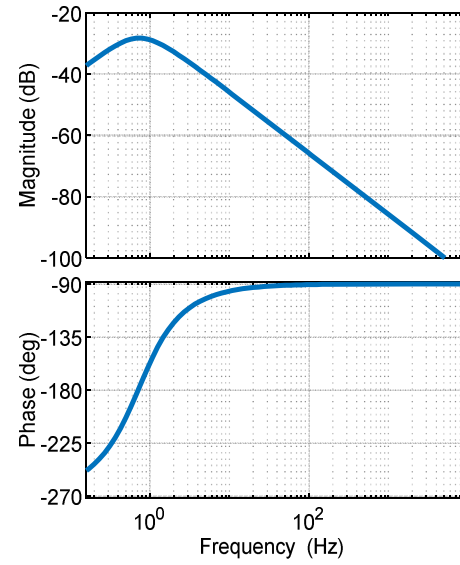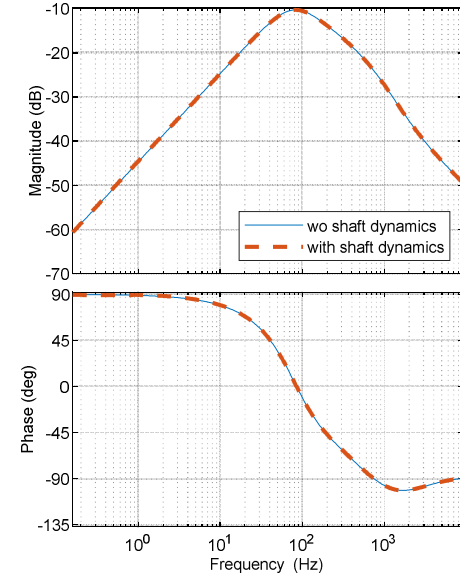

Figure 9 Bode plot of G_{Teq}

Figure 10 Bode plot of Z_{CL}

In summary, all $\mathbf{G}_{de\omega}\mathbf{G}_{Te}$, $G_{v\omega}\mathbf{G}_{Te}$, and $\mathbf{G}_{i\omega}\mathbf{G}_{Te}$ mentioned above are so small that $\mathbf{M}_1$ can be approximated as $\mathbf{M}_2$, indicating the shaft dynamics' impact on the generator-rectifier output impedance is negligible in the presence of AFE, as is shown in Fig. 10. The outer voltage control loop also results in a small impedance gain at low frequency, which further reduces the potential instability due to shaft dynamics, because it keeps the source away from interactions with the load subsystem. To verify the conclusion, a load step at the dc side with 20% power reduction is added. The dc bus voltage responses with and without considering shaft dynamics have the same response, as shown in Fig. 11.
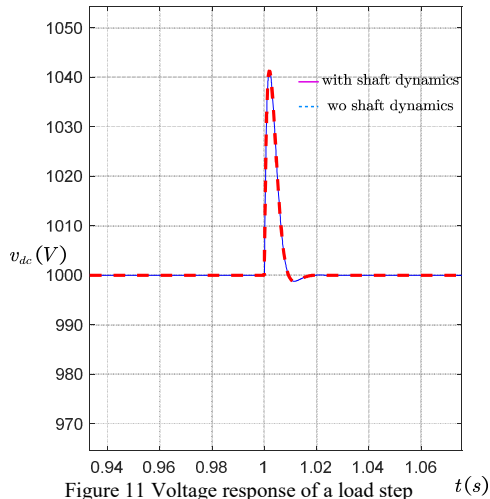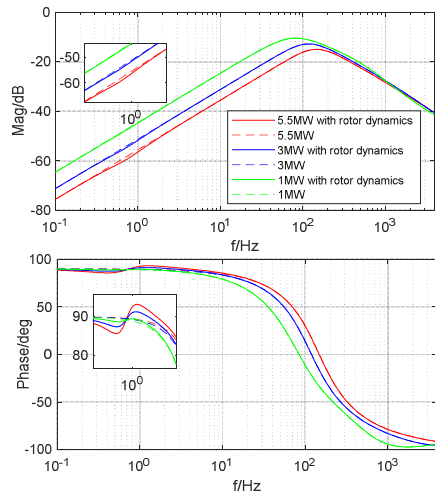
3522

Figure 11 Voltage response of a load step

Figure 12 Output impedance of generator at different power level

IV. IMPACT OF DISTRIBUTED PROPULSION RATIO

Part of the electrical power extracted from the turbofan is transferred to the dc bus and mostly to the tail fan motor to provide distributed propulsion. A highly distributed propulsion ratio is beneficial to increasing aerodynamic efficiency [11]. The turbine model used here can provide around 6MW electrical power if assuming a 100% distributed propulsion. Considering that a larger distributed propulsion ratio may impact the turbine-generator behavior from a stability point of view, a comparison study on different distributed propulsion ratio is carried out. Here generator model rated at different power level, namely 1MW, 3MW, and 5.5MW to represent 16%, 50%, and 90% distributed propulsion, all are tuned to have 100Hz voltage loop bandwidth and 60° phase margin. Fig. 12 shows the output impedance of these three cases. When the distributed propulsion ratio increases, the turbofan shaft dynamics have more impact on the output impedance below 10Hz. Although the impact is still small and not likely to trigger dynamics interactions with load subsystems.

V. CONCLUSIONS

This paper provides a detailed small-signal model of the turbine-generator-rectifier system and analyzes the shaft dynamics' impact on the system output impedance. It reveals AFE can mitigate the impact of shaft dynamics for the following reasons: the speed perturbation has a small impact on the dc bus voltage and stator inductor current; the decoupling terms in the current controller attenuate the speed perturbation impact; the dc voltage control reduces the impedance gain at low frequency. With a larger ratio of distributed propulsion to total propulsion, shaft dynamics tends to have more impact on the source output impedance, though it's still not too significant to cause stability problem. In practice, impedance-measurement-unit can be used to measure the small-signal impedance of the system, to assess the stability condition of the system and verify the conclusions presented in this paper.

REFERENCES

[1] Xiaolong Zhang, Cheryl L. Bowman, Tim C. O'Connell, Kiruba S. Haran, "Large Electric Machines for Aircraft Electric Propulsion," in IET Electric Power Applications, vol. 12, no. 6, p. 767 – 779, July 2018.

[2] P. Wheeler and S. Bozhko, "The More Electric Aircraft: Technology and challenges.," in IEEE Electrification Magazine, vol. 2, no. 4, pp. 6-12, Dec. 2014.

[3] J. W. Connolly, J. W. Chapman, E. J. Stalcup, K. R. Hunker, A. K. Chicatelli and G. L. Thomas, "Modeling and Control Design for a Turboelectric Single Aisle Aircraft Propulsion System," 2018 AIAA/IEEE Electric Aircraft Technologies Symposium, Cincinnati, OH, USA, 2018, pp. 1-19.

[4] Dyson, Rodger W. "NASA Electric Aircraft Testbed (NEAT) Single-aisle Transport Air Vehicle Hybrid Electric Tail-cone Thruster Powertrain Configuration and Test Results." In 2018 AIAA/IEEE Electric Aircraft Technologies, pp. 1-19. IEEE, 2018.

[5] Xiaogang Feng, Jinjun Liu and F. C. Lee, "Impedance specifications for stable DC distributed power systems," in IEEE Transactions on Power Electronics, vol. 17, no. 2, pp. 157-162, March 2002.

[6] F. Gao and S. Bozhko, "Modeling and Impedance Analysis of a Single DC Bus-Based Multiple-Source Multiple-Load Electrical Power System," in IEEE Transactions on Transportation Electrification, vol. 2, no. 3, pp. 335-346, Sept. 2016.

[7] R. D. Middlebrook, "Input filter considerations in design and application of switching regulators," in Proceedings of IEEE Industry Application Society Annual Meeting, Oct. 1976, pp. 94–107.

[8] B. Wen, R. Burgos, D. Boroyevich, P. Mattavelli and Z. Shen, "AC Stability Analysis and dq Frame Impedance Specifications in Power-Electronics-Based Distributed Power Systems," in IEEE Journal of Emerging and Selected Topics in Power Electronics, vol. 5, no. 4, pp. 1455-1465, Dec. 2017.

[9] A. A. A. Radwan and Y. A. I. Mohamed, "Linear Active Stabilization of Converter-Dominated DC Microgrids," in IEEE Transactions on Smart Grid, vol. 3, no. 1, pp. 203-216, March 2012.

[10] R. P. Burgos, P. Kshirsagar, A. Lidozzi, F. Wang and D. Boroyevich, "Mathematical Model and Control Design for Sensorless Vector Control of Permanent Magnet Synchronous Machines," in 2006 IEEE Workshops on Computers in Power Electronics, Troy, NY, 2006, pp. 76-82.

[11] Jeffryes W. Chapman and Jonathan S. Litt, "Control Design for an Advanced Geared Turbofan Engine," in 53rd AIAA/SAE/ASEE Joint Propulsion Conference, AIAA 2017-4820. July 2017.